Effects of electroweak symmetry breaking on axionlike particles as dark matter

Soumen Kumar Manna[*] and Arunansu Sil[†]

Department of Physics, Indian Institute of Technology Guwahati, Assam-781039, India

(Received 13 November 2023; accepted 4 May 2024; published 23 May 2024)

Axionlike particles (ALPs), the pseudo Nambu-Goldstone bosons associated to the spontaneous breaking of global symmetry, have emerged as promising dark matter candidates. Conventionally, in the context of misalignment mechanism, the nonthermally produced ALPs happen to stay frozen due to Hubble friction initially, and at a later stage, they begin to oscillate (before matter-radiation equality) at characteristic frequencies defined by their masses and behaving like cold dark matter. In this work, we study the influence of electroweak symmetry breaking (EWSB), through a higher order Higgs portal interaction, on the evolution of ALPs. Such an interaction is found to contribute partially to the ALP's mass during EWSB, thereby modifying oscillation frequencies during EWSB as well as impacting upon the existing correlation between the scale of symmetry breaking and their masses. The novelty of the work lies in broadening the relic satisfied parameter space so as to probe it in near future via a wide range of experiments.

DOI: 10.1103/PhysRevD.109.095036

I. INTRODUCTION

Axionlike particles (ALPs) are generically classified as the pseudo Nambu-Goldstone bosons (pNGB) associated to the spontaneous breaking of a global symmetry, prevalent in many extensions of the Standard Model (SM), e.g., in superstrings theories [1–3]. Though they are analogous to the pNGB of the $U(1)$ Peccei Quinn symmetry, originally introduced to solve the strong CP problem of QCD [4–7], ALPs belong to a more general class and hence, not necessarily be connected to the solution of the strong CP problem. They are typically very light, neutral pseudoscalar particles having at most a derivative coupling with the Standard Model at an effective level, suppressed by the scale of spontaneous symmetry breaking (f_a) of the global symmetry (also referred to as the ALP decay constant), thereby emerging as ideal candidates for explaining the dark matter of the Universe. The mass of an ALP may originate from nonperturbative instanton effect in a strongly interacting hidden sector (analogous to the QCD axion) as well as from explicit symmetry breaking. Correspondingly, contrary to the QCD axion, an ALP does not in general carry any specific relation between its mass and the decay constant. As a result, their mass and decay constant may span over a wide range making them attractive from detection point of view.

Most commonly in the literature, an ALP is considered to be produced nonthermally via the so-called *misalignment* mechanism [8–12]. The ALP, considered as a classical field in this context, is expected to have an initial nonzero field value and gets frozen there till the Hubble ($\mathcal{H}$) induced friction remains larger that its mass (m_a). Once $\mathcal{H} \sim m_a$, the ALP starts to oscillate at a temperature $T_{\rm osc}$ about the minimum of a periodic potential characteristics of a pNGB. Such an oscillatory field mimics as cold dark matter as the associated energy density (ρ_a) scales as R^{-3}; hence, behaving like ordinary matter (R is the scale factor of the Universe) provided it remains stable over cosmological time scale. The relic density satisfaction of such ALP provides a standard correlation involving m_a and f_a, which turns out to be well restricted by several cosmological constraints as well from ALP search experiments as summarized in [12–16]. Considering all such aspects, it turns out that the ALPs being DM should be very light (below keV).

In this work, we propose to include a higher order shift symmetry breaking Higgs portal interaction of ALPs which contributes to its mass (m_{aE}) after the electroweak symmetry breaking (EWSB) on top of its existing mass, m_{a0}, presumably followed from the nonperturbative instanton effect. Inclusion of such additional mass m_{aE} is expected to modify the frequency of ALP oscillation after the EWSB. This would have profound effect on the relic density and hence, on the ALP parameter space in m_a, f_a plane, where

[*]skmanna2021@gmail.com
[†]asil@iitg.ac.in

$m_a^2 = {m_{a0}}^2 + {m_{aE}}^2$. We find that depending upon the onset of conventional ALP oscillation (connected with its mass m_{a0} only) before or after the EWSB and associated modification of it after EWSB, the standard correlation between ALP mass and decay constant can be altered significantly leading to opening up of otherwise excluded (restricted) parameter space (e.g., keV–GeV range) for ALPs.

There are some studies focusing on modification of the PQ axion or ALP potential. For example, in Ref. [17], the authors examine the effect of tiny (limited by neutron electric dipole moment) explicit Peccei-Quinn (PQ) symmetry breaking on the PQ axion dynamics and its role as DM. In this case, the PQ axion initially starts oscillating about a wrong minimum guided by the explicit PQ breaking term and afterward it oscillates about the true minimum leading to a modification of the conventional PQ parameter space. Reference [18] recently analyzes the effect of introducing a PQ breaking term on axiverse that encompasses the PQ axion, an ALP, and a hypothetical mixing between them. In another work, Ref. [19] discusses the effect of adding a nonperiodic potential to ALP and thereby find the possibility of accommodating a large misalignment angles which may change the conventional (m_a, f_a) parameter space of ALPs. Another modification of axion or ALP potential is referred as *kinetic misalignment* ([20–22]). In this scenario, a higher dimensional explicit PQ breaking potential and a large initial field value for the PQ symmetry breaking field lead to a nonzero initial ALP velocity which in turn, triggers a delayed ALP oscillation bringing modifications in the relic abundance as well as in parameter space of ALPs. A more general treatment of the effect of initial conditions of ALP and its effects on the (m_a, f_a) parameter space can be found in Ref. [23]. Reference [24] discusses about the impact of ALP mass modification on its relic abundance, within the context of the type-II seesaw mechanism.

Our proposal differs from the existing works in a sense that it relies on the electroweak symmetry breaking phase (most natural and unavoidable phase) for modifying the ALP potential, without changing its minimum though. The new mass term for ALP that originates at EWSB may provide a dominant or subdominant contribution to the effective final mass of the ALP (m_a). Depending on the onset of ALP oscillation before or at EWSB, the standard misalignment mechanism gets modified so as to obtain a new parameter space, in (m_a, f_a) plane, carrying significant differences with the standard one, which might be interesting from ALP search experiments. It turns out that such a Higgs portal interaction of ALPs allows us to probe for light ALPs. Interactions involving ALP and Standard Model (SM) Higgs bosons have also been exercised in few references [25–27], however in different contexts. Specifically, a higher dimensional operator consisting of axion and Higgs bosons are discussed in [27], which is responsible for a new minimum of ALP inducing an epoch of kination and generation of gravitational waves. Contrary to our proposal, the ALP there neither plays the role of DM nor obtains a shift in its mass during EWSB.

The outline of the work is as follows. In the next section, we discuss the standard ALP scenario and following this, we move for studying the evolution of ALPs in our modified scenario. The observation and constraints are elaborated in Secs. III and IV, respectively. Finally, we conclude in Sec. VI.

II. STANDARD MISALIGNMENT MECHANISM AND ALP AS DM

In this section, we first elaborate on the production of ALPs in the early Universe via misalignment mechanism followed by standard ALP cosmology and the related parameter space. We presume the existence of ALPs prior to the end of primordial inflation as a result of spontaneous breaking of a global $U(1)$ symmetry during inflation. After inflation (followed by a reheating era), the ALP field $a(\mathbf{x}, t)$ is expected to be spatially homogeneous, hence described by $a(t)$ only, and gets frozen at an initial value a_I parametrized by the misalignment angle $\theta_I = a_I/f_a$ (with $\dot{\theta}_I = 0$), as long as the Hubble remains larger compared to its mass m_{a0}. Note that, the ALP being a Nambu Goldstone Boson, the origin of m_{a0} is related to the breaking of shift symmetry which can possibly be connected to the nonperturbative dynamics, (analogous to PQ axion) and independent of temperature. This can be realized if the ALP couples to a hidden $SU(N)$ sector [the global $U(1)$ symmetry is anomalous under such non-Abelian group], which may not be thermalized.

The related ALP potential can be parametrized by

$$V_0 = m_{a0}^2 f_a^2 \left(1 - \cos\frac{a}{f_a}\right), \tag{1}$$

where f_a corresponds to the scale of spontaneous symmetry breaking of the global $U(1)$. The ALP field a parametrized by $\theta = a/f_a$ follows the classical equation of motion in the background of expanding Universe as given by

$$\ddot{\theta} + 3\mathcal{H}(T)\dot{\theta} - \frac{\nabla^2\theta}{R^2} + \frac{1}{f_a^2}\frac{\partial}{\partial\theta}V_0 = 0, \tag{2}$$

and "dot" indicates the derivative with respect to time t.

At very early Universe, after inflation, when $\mathcal{H} \gg m_{a0}$, the *mode* of the axion field remains overdamped and gets stuck at its initial value θ_I due to Hubble friction. In a radiation dominated era, at some point when

$$3\mathcal{H}(T^0_{\rm osc}) = m_{a0}, \tag{3}$$

the field rolls toward its potential minimum and starts to oscillate. The onset of oscillation can be characterized by

the temperature $T^0_{\rm osc}$. Near the minimum of the potential, $V_0 \simeq \frac{1}{2} {m_{a0}}^2 f_a^2 \theta^2$ and the equation of motion (below $T \lesssim T^0_{\rm osc}$) reduces to

$$\ddot{\theta} + 3\mathcal{H}(T)\dot{\theta} + m_{a0}^2 \theta = 0, \tag{4}$$

where the ALP field is considered to be a homogeneous one, i.e., the spatial variation over Hubble volume, $\nabla^2\theta/R^2$ vanishes. Using the expression of the Hubble parameter $\mathcal{H}$ in a radiation-dominated universe, $\mathcal{H}(T) = 1.66\sqrt{g_\star(T)}T^2/M_{\rm Pl}$, and the relation in Eq. (3), we can estimate the conventional oscillation temperature $T^0_{\rm osc}$ for ALP as

$$T^0_{\rm osc} \simeq 1.5 \times 10^7 \text{ GeV} \left(\frac{100}{g_\star(T^0_{\rm osc})}\right)^{1/4} \left(\frac{m_{a0}}{10^{-3}\text{ GeV}}\right)^{1/2}, \tag{5}$$

where, $g_\star(T)$ is the number of relativistic degrees of freedom (d.o.f) at a temperature T and the value of Planck mass, $M_{\rm Pl} = 1.22 \times 10^{19}$ GeV is deployed.

At the conventional oscillation temperature $T^0_{\rm osc}$, the total energy density of the ALP $\rho_a = (\dot{\theta}^2 f_a^2 + m_{a0}^2 f_a^2 \theta^2)/2$ is fully embedded in its potential part only since ALP does not have any initial velocity, $(\dot{\theta}_I = 0)$ and is given by

$$\rho_a(T^0_{\rm osc}) = \frac{1}{2} m_{a0}^2 f_a^2 \theta_I^2. \tag{6}$$

For $T \lesssim T^0_{\rm osc}$, Eq. (4) implies that field would perform fast oscillations with slowly decreasing amplitude, where the average energy density $\langle \rho_a \rangle$ scales as R^{-3} and the equation of state $\omega = \langle p_a \rangle / \langle \rho_a \rangle$ turns out to be zero implying that it behaves like nonrelativistic matter [12,28]. Here, $\langle\rangle$ implies averaging over one complete oscillation.

Since the ALP number density in a comoving volume turns out to be conserved [12], the present day ALP energy density can be estimated as

$$\rho_a(T_0) = \rho_a(T^0_{\rm osc}) \frac{m_a(T_0)}{m_{a0}(T^0_{\rm osc})} \left(\frac{R_{\rm osc}}{R_0}\right)^3 \tag{7}$$

$$= \frac{1}{2} m_{a0}(T^0_{\rm osc}) m_a(T_0) f_a^2 \theta_I^2 \left(\frac{R_{\rm osc}}{R_0}\right)^3, \tag{8}$$

where $T_0 = 2.4 \times 10^{-4}$ eV is the present temperature and a change of ALP mass at different (later) temperature, if any, is included in the form of $m_a(T)$. However as stated above, unlike QCD Axion, ALP masses are generally considered as temperature independent, i.e.,$m_{a0}(T^0_{\rm osc}) = m_a(T_0) = m_{a0}$. In this case, employing Eq. (8) and considering the adiabatic expansion of the Universe, i.e., $(R_{\rm osc}/R_0)^3 = s(T_0)/s(T^0_{\rm osc})$, where s is the entropy density of the Universe given by $s(T) = (2\pi^2/45) g_{\star s} T^3$, the ALP relic density can be expressed as

$$\Omega_a h^2 = \frac{h^2}{2\rho_{c,0}} m_{a0}^2 f_a^2 \theta_I^2 \left(\frac{g_{\star s}(T_0)}{g_{\star s}(T^0_{\rm osc})}\right) \left(\frac{T_0}{T^0_{\rm osc}}\right)^3, \tag{9}$$

where $\rho_{c,0} = 1.05 \times 10^{-5} h^2$ GeV cm^{-3} (present critical energy density) and $g_{\star s}(T_0) = 3.94$ (number of relativistic d.o.f. at present temperature) [29]. Using the expression of Eq. (5) into Eq. (9), the ALP relic density can be estimated as

$$\Omega_a h^2 \simeq 0.12 \left[\frac{\theta_I}{\mathcal{O}(1)}\right]^2 \left[\frac{100}{g_\star(T^0_{\rm osc})}\right]^{\frac{1}{4}} \times \left[\frac{m_{a0}}{10^{-9}\text{ GeV}}\right]^{\frac{1}{2}} \left[\frac{f_a}{4 \times 10^{11}\text{ GeV}}\right]^2, \tag{10}$$

from which a correlation between the two parameters m_{a0} and f_a can easily be obtained. However, once the astrophysical and cosmological bounds are imposed (to be discussed later in Sec. IV), the allowed mass range for the ALPs falls below keV-scale [30] only.

III. HIGGS PORTAL INTERACTION AND ALP

In this section, we introduce an explicit higher order shift symmetry breaking term in the ALP potential involving the SM Higgs. As a result, a new contribution toward the mass of ALP originates once the electroweak symmetry breaking takes place. The appearance of such a mass term for ALP at an intermediate phase (during its evolution) in addition to m_{a0} (connected to nonperturbative dynamics) not only enables the effective mass of the ALP (m_a) and its decay constant (f_a) to treat as independent parameters, but also modifies the frequency of ALP oscillation at EWSB as we observe below.

We first consider the Lagrangian involving a global $U(1)$ symmetry breaking complex scalar field $\Phi = \eta e^{\theta}/\sqrt{2}$, as

$$\mathcal{L} = \frac{1}{2}(\partial\eta)^2 + \frac{1}{2} f_a^2 (\partial\theta)^2 - \lambda(\eta^2 - f_a^2/2)^2, \tag{11}$$

where $\theta = a/f_a$ as parametrised in the earlier section. Once the $U(1)$ global symmetry is spontaneously broken, the potential for the ALP field a is given V_0 of Eq. (1). We now introduce additional dimension-6 shift symmetry breaking term involving SM Higgs doublet H, as given by

$$V_1 = \frac{|H|^4}{\Lambda^2} \Phi^2 e^{i\alpha} + \text{H.c.}, \tag{12}$$

where the phase α in Eq. (12) can take values in the range $0 \le \alpha \le \pi$ [31] and Λ acts as a cutoff scale with $\Lambda > f_a$, indicating that the explicit breaking of the global symmetry may take place at some high scale ($\Lambda \lesssim M_{\rm Pl}$) [32,33]. Based on this known possibility that gravity effects explicitly break a global symmetry [34–38] at Planck scale $M_{\rm Pl}$ (or even at a scale much smaller than the Planck one, as recently shown by [33] in the context of weak-gravity

conjecture [39]), we discuss the origin of such an operator in Appendix A. The specific construction mentioned there is also capable of disallowing another dimension-6 explicit $U(1)$ symmetry breaking term $\frac{|H|^2}{\Lambda^2}\Phi^4\exp(i\alpha)+\text{H.c.}$, which can be present otherwise. Note that this additional operator can be excluded from a naive consideration too by keeping the order of explicit $U(1)$ breaking [by amount of $U(1)$ charges] minimal. While we mostly focus on the explicit breaking operator as in Eq. (12) only for the rest of the analysis, we show in Appendix B that inclusion of the additional dimension-6 operator may lead to an altogether different phenomenology.

The phenomenologically relevant part of the potential for the ALP or the θ field, after the spontaneous breaking of the PQ-like global symmetry, then turns out to be

$$V_a = m_{a0}^2 f_a^2\left(1-\cos\frac{a}{f_a}\right)+\frac{|H|^4}{\Lambda^2}f_a^2\cos\left(\frac{2a}{f_a}+\alpha\right). \quad (13)$$

At a temperature sufficiently higher than the electroweak scale, $T > T_{\rm EW}\sim 150$ GeV, the temperature correction to the SM Higgs potential helps the SM Higgs boson to have a single minimum at origin [40]. Hence the Higgs field is expected to settle at origin as a result of which this term does not contribute till the temperature becomes comparable to $T_{\rm EW}$ when H gets a vacuum expectation value (vev), $H=(v+h)/\sqrt{2}$ with $v=246$ GeV. After the EWSB, the ALP receives a new contribution to its mass such that its effective mass m_a satisfies the relation,

$$m_a^2 \equiv \left(\frac{d^2V_a}{da^2}\right)_{\rm min} = m_{a0}^2\cos\theta_{\rm min}-\frac{v^4}{\Lambda^2}\cos(2\theta_{\rm min}+\alpha), \quad (14)$$

where $\theta_{\rm min}=a_{\rm min}/f_a$ denotes the newly developed minimum of the ALP potential after EWSB. The value of $\theta_{\rm min}$ can be estimated as a solution to the equation,

$$\sin\theta=\frac{q}{2}\sin(2\theta+\alpha), \quad \text{with} \quad q=\frac{v^4/\Lambda^2}{m_{a0}^2}, \quad (15)$$

obtained by minimising the ALP potential. Clearly, the new potential minimum depends on the choice of α and other parameters (Λ and m_{a0}). We pursue with $\alpha=\pi$ for the rest of the analysis that results into the effective mass of the ALP given by

$$m_a^2 = m_{a0}^2+\frac{v^4}{\Lambda^2}. \quad (16)$$

Such a choice of $\alpha=\pi$ is motivated primarily from the fact that the minimum of the ALP potential ($\theta_{\rm min}=0$) remains unaffected due to the presence of this additional contribution to ALP potential via Eq. (12). However, for conventional QCD axion, such explicitly breaking term should be incorporated very carefully as any alteration of the minimum can spoil the resolution of the strong CP problem, the strong-CP violating angle being heavily constrained by neutron electric dipole moment [41] (widely referred as axion quality problem [42–44]). With general axionlike particles, such a solution of strong CP problem is not necessarily be connected to the solution of the strong CP problem. To investigate the impact of different α values on $\theta_{\rm min}$ and hence on relic, we incorporate an analysis in the later part of the following subsection.

Appearance of such a mass term would affect the evolution of the ALP field, in terms of its change in oscillation frequency, immediately after the EWSB. To analyze it further, we divide the study into two cases depending on whether the ALP starts its oscillation at a temperature $T_{\rm osc}^0$ (due to m_{a0}) prior to EWSB temperature $T_{\rm EW}$ or not, as

$$\begin{aligned}&\text{Case[A]}:\ T_{\rm osc}^0 > T_{\rm EW},\\ &\text{Case[B]}:\ T_{\rm osc}^0 \le T_{\rm EW}.\end{aligned} \quad (17)$$

Note that the demarcation between these two cases is set by the condition,

$$m_{a0} = 3\mathcal{H}(T_{\rm EW}), \quad (18)$$

which translates (assuming a radiation dominated universe) into $m_{a0} > 10^{-13}$ GeV (for case [A]) and $m_{a0}\le 10^{-13}$ GeV (for case [B]), where we use $T_{\rm EW}=150$ GeV.

A. ALP oscillation starts before EWSB

Here, the ALP is expected to start its oscillation at a temperature $T_{\rm osc}^0$ higher than $T_{\rm EW}$, connected to its mass m_{a0}. So, the evolution of this ALP for the period $T_{\rm osc}^0$ to $T_{\rm EW}$ is guided by Eq. (4). Near the onset of its oscillation at $T=T_{\rm osc}^0$, it carries an energy density same as of Eq. (6). At $T=T_{\rm EW}$, due to the electroweak symmetry breaking, the higher order Higgs portal interaction provides an additional contribution to its mass as specified in Eq. (16). As a result, the evolution of the ALP is now governed by the same form of Eq. (4), however replacing m_{a0} by m_a via Eq. (16), i.e.,

$$\ddot{\theta}+3\mathcal{H}(T)\dot{\theta}+m_a^2\theta=0. \quad (19)$$

The shift of ALP mass across the EWSB can be incorporated in estimating the ALP energy density ρ_a, crucial in determining the ALP relic density, before and after the electroweak phase transition in line with the discussion in the context of Eqs. (7) and (8) as pursued below. The discontinuity of m_a around EWSB can be guided by an appropriate logistic function (as shown in Appendix C) in case one tries to explore evolution of the θ field as function of scale factor R (normalized by R_0), depicted in Fig. 1.

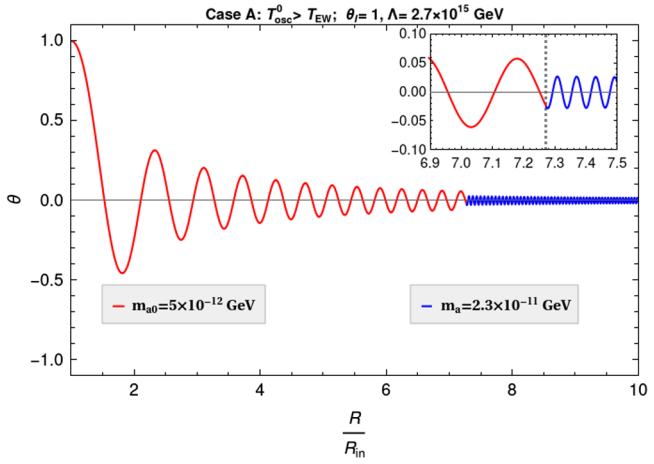

FIG. 1. Evolution of θ before EWSB (solid red) and after EWSB (solid blue) against $R/R_{\rm in}$ in case A ($T^0_{\rm osc} > T_{\rm EW}$). In the inset, the evolution of θ is shown in the vicinity of $T_{\rm EW}$ (the dashed gray vertical gridline of the inset diagram corresponds to $T_{\rm EW}$).

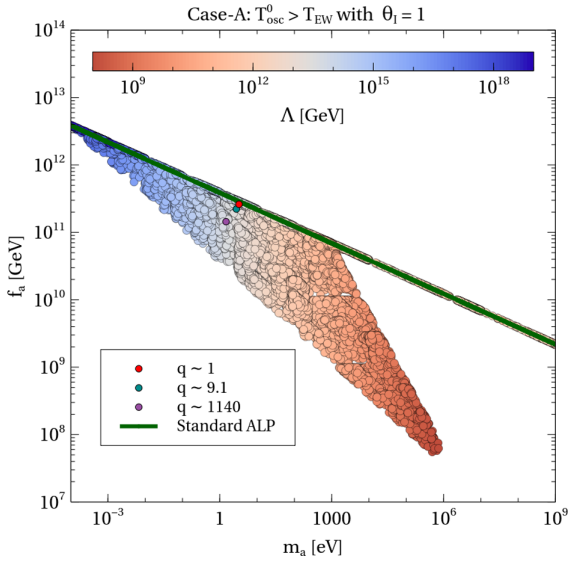

FIG. 2. Relic satisfied parameter space comparison between case A ($T^0_{\rm osc} > T_{\rm EW}$) and standard case in ($m_a - f_a$) plane, while variation of Λ is shown in the color bar. The bold dots in red, dark cyan, and purple are points taken for studying further dependence of $\theta_{\rm min}$ on α.

Considering the conservation of ALP number density in a comoving volume across EWSB, the ρ_a immediately after the EWSB (at $T_{<\rm EW}$) can be written, via Eq. (7), as

$$\rho_a(T_{<\rm EW}) = \rho_a(T_{>\rm EW})\left(\frac{R_>}{R_<}\right)^3\left[\frac{m_a(T_{<\rm EW})}{m_a(T_{>\rm EW})}\right]. \quad (20)$$

Here, $\rho_a(T_{>\rm EW})$ is the energy density of the ALP just before the EWSB (at $T_{>\rm EW}$) given by

$$\rho_a(T_{>\rm EW}) = \rho_a(T^0_{\rm osc})\left(\frac{R_{\rm in}}{R_>}\right)^3, \quad (21)$$

where $R_{\rm in}$ is the scale factor at the onset of oscillation, $T^0_{\rm osc}$. While the mass of the ALP before EWSB is $m_a(T_{>\rm EW}) = m_{a0}$, $m_a(T_{<\rm EW}) = m_a$ results after EWSB as given by Eq. (16). Here, $R_>$ and $R_<$ are the scale factors of the Universe at temperatures $T_{>\rm EW}$ and $T_{<\rm EW}$, respectively.

The energy density of the ALP today (associated with temperature T_0) can be written as

$$\begin{aligned}\rho_a(T_0) &= \rho(T_{<\rm EW})\left(\frac{R_<}{R_{\rm To}}\right)^3 \\ &= \rho_a(T^0_{\rm osc})\frac{m_a}{m_{a0}}\left[\frac{g_{\star s}(T_0)}{g_{\star s}(T^0_{\rm osc})}\right]\left(\frac{T_0}{T^0_{\rm osc}}\right)^3, \end{aligned} \quad (22)$$

where Eqs. (20) and (21) are employed and $R_{\rm To}$ corresponds to today's scale factor.

Using the expressions of $\rho_a(T^0_{\rm osc})$ of Eq. (6), $T^0_{\rm osc}$ as given by Eq. (5) and plugging them in $\rho_a(T_0)$ of Eq. (22), we find the ALP relic density today as

$$\begin{aligned}\Omega_a h^2 \simeq 0.12&\left(\frac{\theta_I}{1}\right)^2\left(\frac{100}{g_\star(T^0_{\rm osc})}\right)^{1/4} \\ &\times\left(\frac{m_a}{6\times10^{-8}\ {\rm GeV}}\right)\sqrt{\frac{10^{-9}\ {\rm GeV}}{m_{a0}}}\left(\frac{f_a}{5\times10^{10}\ {\rm GeV}}\right)^2. \end{aligned} \quad (23)$$

Apart from m_{a0}, the m_a dependence relies on the cutoff scale Λ. Unlike the standard dependence of relic on m_{a0} and f_a via Eq. (10), here in case-[A], the final relic density also involves the third parameter Λ, the cutoff scale of the theory which is apparent though the involvement of m_a in Eq. (23) apart from m_{a0}.

The effective mass m_a being the final mass of the ALP which is phenomenologically more relevant than m_{a0}, we choose to consider the three parameters as m_a, f_a, and Λ for our phenomenological analysis. To make the parameters dependence of the relic density explicit, we provide the result of the parameter space scan in $m_a - f_a$ plane shown in Figs. 2 and 3, where the dependence of Λ and m_a/m_{a0} are indicated in the respective color maps maintaining $f_a \le \Lambda \le M_{\rm Pl}$. All the points in m_a and f_a plane satisfy the correct relic density $\Omega_a h^2 \simeq 0.12$ [45]. The gradients of the colors inside the color maps ranging from dark red to blue (for Fig. 2) and yellow to brown (for Fig. 3) indicate the one to one correspondence between the $\{m_a, f_a\}$ set of values with Λ and m_a/m_{a0}, respectively, for case-[A]. The narrow green line (merged with the borderline of the parameter space of Figs. 2 and 3) represents the relic-satisfied parameter space for standard scenario with ALP mass, equivalent to m_a, from the very beginning. To clarify

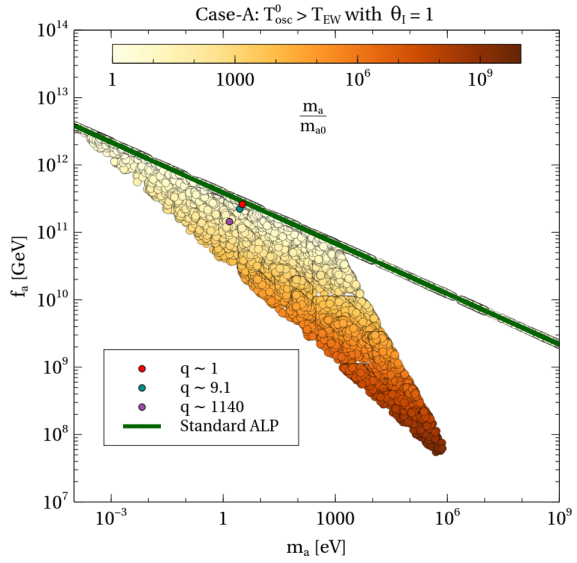

FIG. 3. Relic satisfied parameter space comparison between case A ($T^0_{\rm osc} > T_{\rm EW}$) and standard case in ($m_a - f_a$) plane, while variation of m_a/m_{a0} is shown in the color bar.

further, for the green line only, the ALP oscillation begins at some other temperature (say T_*) than $T^0_{\rm osc}$ satisfying $3\mathcal{H}(T_*) = m_a(T_*)$. In terms of the extended parameter space as obtained in our scenario, this green line acts as the borderline of the parameter space implying that on this line, the change in the ALP mass during EWSB (in presence of the Higgs portal interaction) in very negligible i.e. $m_a/m_{a0} \simeq 1$, which is clear from Fig. 3. Interestingly, the rest of the extended region allows for a significant gain in ALP mass during EWSB, e.g. $m_a/m_{a0} \sim \mathcal{O}(10^9)$ for $\{m_a, f_a\} = \{10^{-3}, 5 \times 10^7\}$ GeV, as evident from the top-color-bar of Fig. 3.

Note that, the presence of the higher dimensional Higgs portal coupling of the ALP allows such broadening of parameter space (particularly for f_a) which would be very significant from experimental perspective clubbed with other constraints which we shall discuss in the next sec. IV. The broadening of the parameter space is an artifact of intermediate change in ALP oscillation frequency as shown in Fig. 1. Considering the ALP to constitute 100% of dark matter energy density in the universe, the upper part of the parameter space in this case (which is merged with the standard case) is excluded by the overabundance of dark matter while the excluded region below this (the left and right border lines of the allowed parameter space) is due to the consideration: $\Lambda > f_a$. In terms of ALP mass, the lower limit on m_a is kept as 10^{-13} GeV here so as to keep $T^0_{\rm osc}$ above $T_{\rm EW}$, the higher side of m_a can even be extended beyond the specified value (1 GeV) of the figure. The other constraint, $\Lambda < M_{\rm Pl}$ is only important at the leftmost region of the parameter space in this case as the minimum contribution from dim-6 operator to ALP mass is $\simeq v^2/M_{\rm Pl} = 5 \times 10^{-15}$ GeV. However, such a correlation involving m_a and the decay constant f_a deserves a further scrutiny from several astrophysical and cosmological bounds which we will discuss in a subsequent section.

It is perhaps pertinent here to comment on the choice of the phase, α. We noted that for the specific choice of $\alpha = \pi$, the $\theta_{\rm min}$ remains at the origin even after the EWSB. However, for an arbitrary α, this may not be the case always, indicating a possible impact on the final relic density of ALP. To investigate this, we first use Eq. (15) to demonstrate the variation of $\theta_{\rm min}$ against α for some choices of q values. For this purpose, we pick up three different sets of parameters $[m_{a0}, f_a, \Lambda]$ (corresponding to three different q values) from the parameter space of Fig. 2 (or 3): (a) $[2.31 \times 10^{-9}, 2.61 \times 10^{11}, 2.62 \times 10^{13}]$ GeV, marked in red dark dot having $q \sim 1$, (b) $[8.74 \times 10^{-10}, 2.22 \times 10^{11}, 2.29 \times 10^{13}]$ GeV, marked in dark cyan dark dot having $q \sim 9.1$, and (c) $[4.35 \times 10^{-11}, 1.44 \times 10^{11}, 4.12 \times 10^{13}]$ GeV, marked in purple dark dot having $q \sim 1140$. We then employ these three q values to obtain $\theta_{\rm min}$ as function of α for each q as depicted in Fig. 4. Firstly, we note that with $\alpha = 0$, the potential minimum in terms of $\theta_{\rm min}$ depends on the choice of q. To be specific, $\theta_{\rm min}$ remains at origin for $q \leq 1$, while it becomes $|\theta_{\rm min}| = \cos^{-1}(1/q)$ for $q > 1$. For nonzero α, $\theta_{\rm min}$ picks a distinct value. Hence, a correlation between $\theta_{\rm min}$ and α is noticed in this case as observed in Fig. 4. However, for $\alpha = \pi$, $\theta_{\rm min}$ turns out to be zero irrespective of q, signifying $\alpha = \pi$ to be an unique choice.

Corresponding to Fig. 4, a variation in relic density with α is shown in Fig. 5. It is evident that a maximum relic density results for $\alpha = \pi$. This is simply because the relic density being proportional to the effective ALP mass attains its maximum value for $\alpha = \pi$ as can be seen from Eq. (15) [or (16)]. Any other choice of α obviously produces a reduced relic density as the resulting mass remains smaller

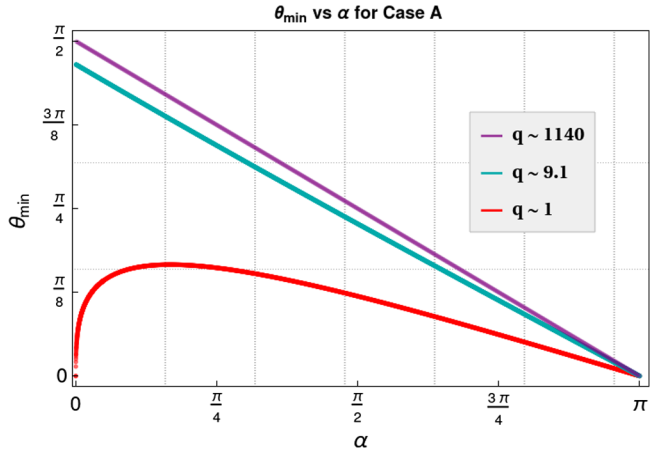

FIG. 4. Variation of ALP potential minimum in terms of $\theta_{\rm min}$ against α. The three lines corresponds to three reference points, taken from the parameter spaces in Figs. 2 and 3 having different values of q.

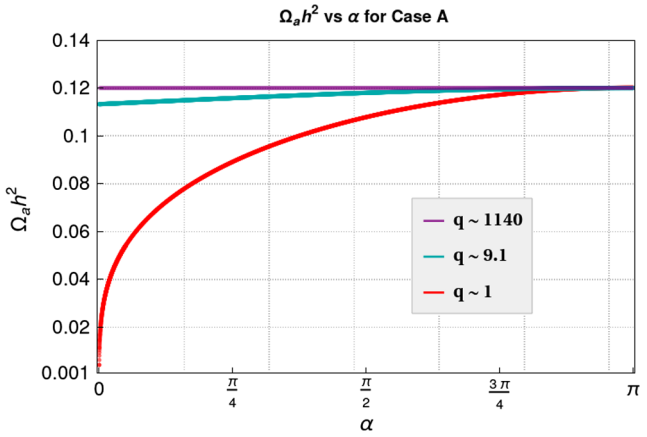

FIG. 5. Variation of the ALP relic density ($\Omega_a h^2$) vs α. The three lines corresponds to three reference points, taken from the parameter spaces in Figs. 2 and 3 having different values of q.

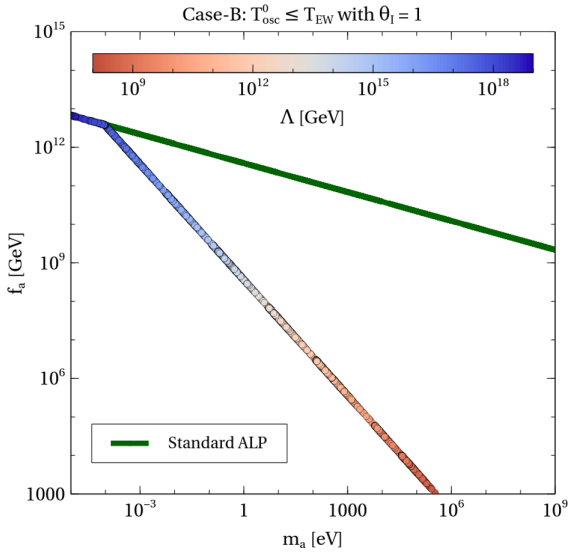

FIG. 6. Relic satisfied parameter space comparison between case B ($T^0_{\rm osc} \leq T_{\rm EW}$) and standard case in ($m_a - f_a$) plane, while variation of Λ is shown in the color bar.

than its maximum value. As indicated in Fig. 5, the change in relic density is only significant for $q \lesssim \mathcal{O}(10)$. For a sizeable q ($v^4/\Lambda^2 \gg m_{a0}^2$), the variation in relic density is almost negligible with $0 \leq \alpha \leq \pi$. However, such a decrease in relic density can also be compensated by appropriate scaling of f_a value which is not directly entering in determining the $\theta_{\rm min}$.

B. ALP oscillation starts after EWSB

Now we elaborate on the possibility where the ALP is scheduled to start its conventional oscillation (connected to its mass m_{a0} only) after EWSB. As discussed earlier, this can materialize only if $m_{a0} < \mathcal{O}(10^{-13})$ GeV. In this case, even if the global symmetry is spontaneously broken during or before inflation, the ALP field got stuck at the misalignment angle θ_I. The situation may alter with the presence of dim-6 Higgs portal interaction we include in this work leading to two possibilities: (a) the effective mass after EWSB m_a immediately satisfies the condition $m_a(T_{\rm EW}) \geq 3\mathcal{H}(T_{\rm EW})$, thanks to the Higgs portal contribution toward m_a; (b) even with the additional contribution to its mass, m_a satisfies the condition $m_a(T) = 3\mathcal{H}(T)$ with a temperature smaller than $T_{\rm EW}$ and hence ALP oscillation starts later.

We notice that contrary to case [A], there would not be any abrupt change in ALP oscillation here as the oscillation begins already with the effective mass at or below EWSB. The evolution of ALP then proceeds according to the Eq. (19). The rest of the prescription for evaluating the final relic is similar to the standard case discussed in the Sec. II. The $m_a - f_a$ parameter space satisfying the final relic for this case is represented in Figs. 6 and 7, while the corresponding values of Λ parameter and the ratio m_a/m_{a0} are shown in top bar, respectively. In the same plot, the standard case (i.e., without Higgs portal coupling) relic satisfied parameter space having ALP mass equivalent of m_a from the beginning is indicated by the green patch for comparison purpose. The relic satisfied parameter space in this case [B] is not broadened (absence of elongated relic satisfied patch as in case [A]) compared to the conventional or standard parameter space as there is no such intermediate change in oscillation frequency. However, the standard ALP parameter space for this range of final ALP mass changes its gradient due to a different onset of ALP oscillation era (it starts at $T_* > T_{\rm EW}$ related to its mass equivalent of m_a). It is found that except for large Λ satisfying $\Lambda \sim \mathcal{O}(M_{\rm Pl})$, the Higgs portal operator provides dominant contribution to ALP final mass, i.e.,

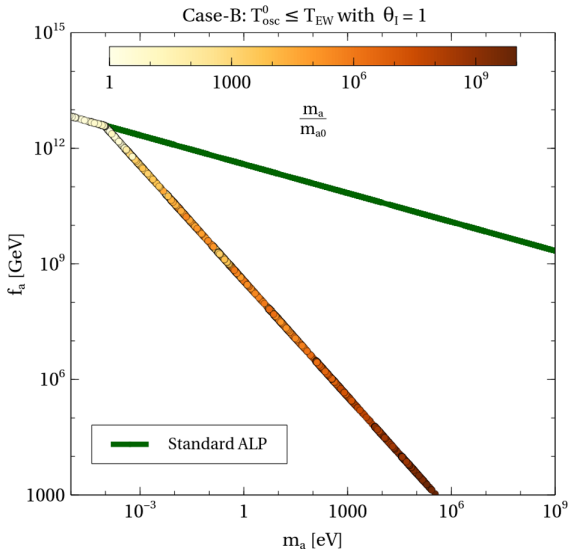

FIG. 7. Relic satisfied parameter space comparison between case B ($T^0_{\rm osc} \leq T_{\rm EW}$) and standard case in ($m_a - f_a$) plane, while variation of m_a/m_{a0} is shown in the color bar.

$m_a = \sqrt{m_{a0}^2 + \frac{v^4}{\Lambda^2}} \simeq \frac{v^2}{\Lambda}$. The minimum contribution to ALP mass obtainable from the dim-6 Higgs portal is of order $v^2/M_{\rm Pl} \simeq 5 \times 10^{-15}$ GeV which sets the boundary of m_a to its lower side. Around this large Λ, both m_{a0} and Higgs portal contributions are comparable (refer to Fig. 7) explaining the overlap of the two parameter space lines near $m_{a0} \sim 10^{-13}$ GeV.

IV. CONSTRAINTS ON ALP PARAMETER SPACE

In the previous section, we analyze the relic satisfied parameter space of ALP characterized by its final mass m_a and the decay constant f_a. However, such a parameter space can be further constrained from astrophysical and cosmological limits as well as few laboratory and telescope searches, provided one considers an ALP-photon coupling [28,46] of the form,

$$\frac{g_{a\gamma\gamma}}{4} F_{\mu\nu}\tilde{F}^{\mu\nu} a, \tag{24}$$

where $F_{\mu\nu}$ and $\tilde{F}^{\mu\nu}$ are the electromagnetic field strength tensor and its dual respectively. The effective coupling $g_{a\gamma\gamma}$ can be written in terms of the ALP decay constant f_a as

$$g_{a\gamma\gamma} = \frac{\alpha}{2\pi f_a} C_{a\gamma\gamma}. \tag{25}$$

Generally, $C_{a\gamma\gamma}$ is expected to be $\mathcal{O}(1)$, and α is the fine-structure constant.

Such an ALP-photon coupling opens up several windows of observation on which a considerable effort is being devoted now-a-days. These ALPs might get produced within the searing plasma of stars via interactions with photons. Such process may subsequently impact the stellar evolution leading to an overall energy loss of a star while escaping. Therefore, the nonobservance of any unwanted energy loss in stars sets bounds on the parameter $g_{a\gamma\gamma}$ [47,48]. A stringent bound on $g_{a\gamma\gamma} < 6.6 \times 10^{-11}$ GeV^{-1} emerges from the study of evolution of the horizontal branch (HB) stars [49]. Also, the Sun is a likely source of ALPs (solar ALP), which are detectable on Earth in a telescope with a macroscopic magnetic field via reverse Primakoff process, commonly known as the *Helioscope* [50]. We have used the latest findings with best sensitivity from the CERN Axion Solar Telescope (CAST), which also puts constraints on $g_{a\gamma\gamma}$ similar to those derived from the study of HB stars as, $g_{a\gamma\gamma} < 6.6 \times 10^{-11}$ GeV^{-1} for $m_a < 0.02$ eV [51]. The ALP-photon interaction is also constrained by the measurements of solar neutrino flux as $g_{a\gamma\gamma} < 7 \times 10^{-10}$ GeV^{-1} for $m_a \lesssim \mathcal{O}$(keV) [52]. Other important constraints emerge from the cavity experiments such as Rochester-Brookhaven-Florida and University of Florida (RBF and UF) and Axion Dark Matter Experiment (ADMX), which are sensitive for the ALP mass ranges of 4.5–16.3 μeV [53–55] and 1.9–3.3 μeV [56], respectively. Telescope searches including Visible Multi-Object Spectrograph (VIMOS) and Multi Unit Spectroscopic Explorer (MUSE) further constrain the ALP mass ranges of 4.5–5.5 eV and 2.7–5.3 eV, respectively [15,57].

Searches for ALP are also actively done by various laboratory experiments. One such experimental approach is the light shining through a wall (LSW) experiment [58], where a laser beam is expected to be converted into axion or ALPs after being exposed to a high magnetic field. Subsequently, these converted particles pass through an opaque wall and upon reconverting into photons via a second magnetic field behind the wall, they provide indirect evidence for the presence of ALPs. The current best limit by such LSW experiments are given by OSQAR (Optical Search for QED Vacuum Birefringence, Axions, and Photon Regeneration) as $g_{a\gamma\gamma} < 3.5 \times 10^{-8}$ GeV^{-1} for $m_a < 0.3$ meV [59].

The cosmological constraint of $\Gamma^{-1}_{a\to\gamma\gamma} \geq \tau_U$ (with τ_U being the age of the Universe and $\Gamma_{a\to\gamma\gamma} = g^2_{a\gamma\gamma} m_a^3/64\pi$ representing the decay width of ALP) serves as a key condition in guaranteeing the stability of the nonthermally produced cosmic ALPs as a viable dark matter over the Universe lifetime [30]. If $\Gamma^{-1}_{a\to\gamma\gamma} < \tau_U$, the extra radiations impart additional limits on $g_{a\gamma\gamma}$ extending to very large ALP masses [60]. Additionally, photons from ALP decays can be seen as peaks on top of the known backgrounds in the galactic x-ray spectra and must not surpass the extragalactic background light (EBL) [61]. Also, ALP decaying into photons can lead to the ionization of primordial hydrogen, and the constraint comes from the requirement to prevent this ionization from making a crucial contribution to the optical depth after recombination and hence, ensuring the consistency of BBN with observations [13,60,62]. Other cosmological constraints comes from the excess photons (when decay occurs during an opaque universe) include spectral distortions in the CMB spectrum and increase in T_γ (photon temperature) relative to T_ν (neutrino temperature), thus modifying the value of $N_{\rm eff}$ inferring from WMAP [62].

The bounds regarding all these constraints are shown in the Fig. 8, which are taken from the updated online repository `AxionLimits` [63]. In Fig. 8, the yellow line acts as the demarkation line below which the ALP may serve as a viable dark matter ($\Gamma^{-1}_{a\to\gamma\gamma} > \tau_U \simeq 10^{17}$ sec). On the other hand, the red line corresponds to the ALP dark matter relic satisfaction contour originating from the standard misalignment mechanism (as discussed in Sec. II) representative of the green line displayed in Figs. 2, 3, 6 and 7 with the consideration of $C_{a\gamma\gamma} = 1$ (which is followed throughout the analysis). The obtained parameter spaces in our scenario (Figs. 2 and 6) of cases [A] and [B] are further constrained by these bounds and the residual allowed parameter regions in $m_a - g_{a\gamma\gamma}$ plane (converted from

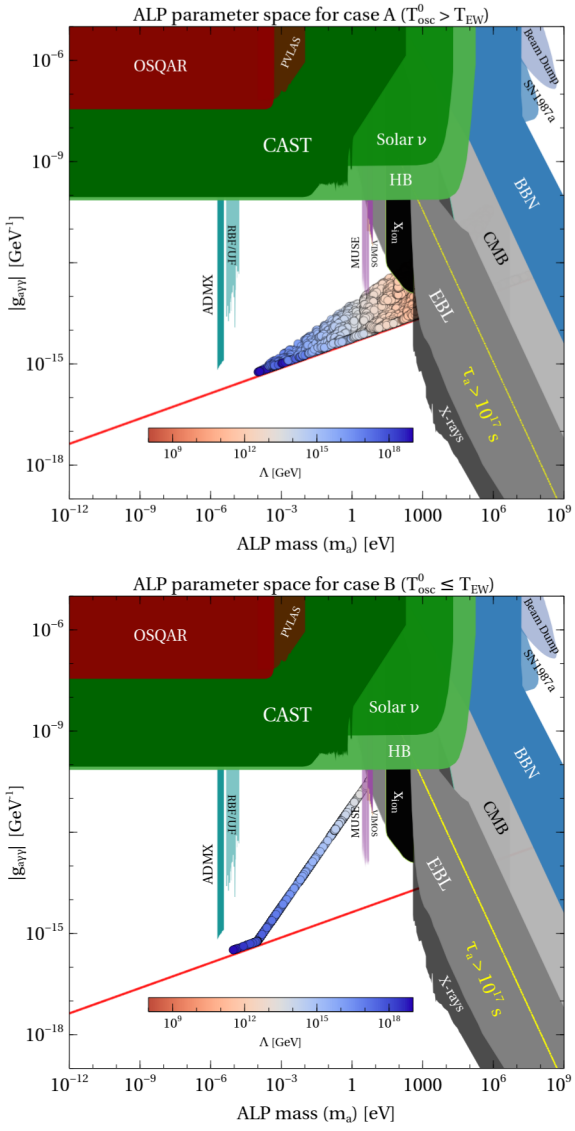

FIG. 8. Excluded regions in ALP parameter space by various constraints along with the relic-satisfied ALP parameter space denoted by dark-red to blue patch for case A (*upper panel*) and blue patch for case B (*lower panel*) in $m_a - g_{a\gamma\gamma}$ plane. The solid red line represents the ALP as DM from conventional misalignment mechanism (with $C_{a\gamma\gamma} = 1$).

$m_a - f_a$) are demonstrated in top and bottom panels of Fig. 8, respectively. Note that as seen from Fig. 8 corresponding to case A, ALP masses ranging from $\mathcal{O}$(keV) to 10^{-13} GeV (serves as the lower limit for this case as per our previous discussion) are allowed with larger couplings (by several orders of magnitude) compared to the conventional picture (red line). Similarly, higher ALP-photon couplings are permitted for case B as well, where the upper limit of allowed ALP mass turns out to be $\mathcal{O}(10)$ eV while the lower limit is set at $m_a \approx 5 \times 10^{-15}$ GeV, which is the minimum mass contribution arising from the dimension-6 operator. It is important to note that for standard misalignment of ALP (without any higher dimensional soft symmetry breaking term), the lower limit of ALP mass can be extrapolated upto very small values ($\sim 10^{-24}$ eV) [28].

V. ISOCURVATURE PERTURBATIONS

In the present scenario, where the PQ-like symmetry is assumed to be broken during inflation, the ALP field should experience quantum fluctuations having an amplitude denoted by $\delta a \simeq \mathcal{H}_{\rm inf}/2\pi (or, \delta\theta_I \simeq \mathcal{H}_{\rm inf}/2\pi f_a)$, where $\mathcal{H}_{\rm inf}$ is the Hubble parameter during inflation. These quantum fluctuations give rise to isocurvature perturbation of the cold dark matter [64–66], which is constrained from the measurements of the CMB anisotropies.[1] The contribution of ALP to CDM isocurvature perturbation $\mathcal{S}_{\rm CDM}$ can be expressed as

$$\mathcal{S}_{\rm CDM} = \frac{\delta\rho_{\rm CDM}}{\rho_{\rm CDM}} = \frac{\Omega_a}{\Omega_{\rm CDM}} \frac{\delta\rho_a}{\rho_a}. \tag{26}$$

In our scenario, ALP contributes entirely to relic density of CDM, i.e., $\Omega_{\rm CDM} = \Omega_a$. The spectrum of CDM isocurvature perturbation in the Fourier space is given by

$$\mathcal{P}_{\rm iso}(k) = (|(\mathcal{S}_{\rm CDM})_k|)^2, \tag{27}$$

k is the comoving wave number, to be evaluated at the pivot scale k_* defined by $k_*/a_0 = 0.05$ Mpc^{-1}. The limit imposed by *Planck* [45] on CDM isocurvature perturbation with respect to the adiabatic power, $\mathcal{P}_{\rm adi}(k_*) \approx 2.2 \times 10^{-9}$, is expressed as [45]

$$\beta_{\rm iso} = \frac{\mathcal{P}_{\rm iso}(k_*)}{\mathcal{P}_{\rm iso}(k_*) + \mathcal{P}_{\rm adi}(k_*)} < 0.038. \tag{28}$$

The ALP density perturbation $\mathcal{S}_{\rm CDM}$ of Eq. (26) can also be recast as

$$\mathcal{S}_{\rm CDM} = 2\frac{\delta\theta_I}{\theta_I}, \tag{29}$$

using $\delta\rho_a/\rho_a \simeq 2\delta\theta_I/\theta_I$ which follows from Eq. (6). Considering the misalignment angle θ_I to be $\mathcal{O}(1)$ and employing the fluctuation of the misalignment angle during inflation, $\delta\theta_I \simeq \mathcal{H}_{\rm inf}/2\pi f_a$, into Eqs. (29) and (27), we obtain

$$\mathcal{P}_{\rm iso} = \left(\frac{\mathcal{H}_{\rm inf}}{\pi f_a}\right)^2 \left(\frac{\mathcal{O}(1)}{\theta_I}\right)^2. \tag{30}$$

Following the constraint in Eq. (28) and considering $\theta_I = 1$ as in the previous sections, we obtain an upper bound on the inflationary Hubble scale $\mathcal{H}_{\rm inf}$ as

$$\mathcal{H}_{\rm inf} < 2.9 \times 10^{-5} f_a. \tag{31}$$

[1]These ALP fluctuations however do not play any role in the overall density fluctuations of the Universe.

Depending on the specific cases in our scenario, we can derive a few more constraints as a consequence of Eq. (31) [12] as we discuss in the following.

For case A ($T^0_{\rm osc} > T_{\rm EW}$), the ALP mass at the onset of oscillation can be constrained by the required condition $3\mathcal{H}_{\rm inf} > 3\mathcal{H}(T^0_{\rm osc}) = m_{a0}$. Using Eq. (31) and setting $\Omega_a h^2 \simeq 0.12$ in Eq. (23), we obtain the following relation:

$$\left(\frac{m_a}{6\times 10^{-8}\ \text{GeV}}\right)\left(\frac{f_a}{5\times 10^{10}\ \text{GeV}}\right)^{3/2} < 6.6\times 10^7, \quad (32)$$

where $g_\star(T^0_{\rm osc}) \simeq 100$ is considered.

On the other hand, for case B ($T^0_{\rm osc} \leq T_{\rm EW}$), the constraints can appear in two different ways: (i) when the ALP with effective mass m_a starts to oscillate at $T = T_{\rm EW}$ only, the criteria $3\mathcal{H}_{\rm inf} > 3\mathcal{H}(T_{\rm EW})$ along with Eq. (31) leads to

$$f_a > 1.08\times 10^{-9}\ \text{GeV}. \quad (33)$$

(ii) Secondly, if the oscillation temperature of the ALP with effective mass m_a is itself smaller than $T_{\rm EW}$ (no intermediate change in the ALP mass takes place), we need to utilize the criteria $3\mathcal{H}_{\rm inf} > m_a$. Here, similar to case A, using Eq. (31) and setting $\Omega_a h^2 \simeq 0.12$ in Eq. (10) (with m_{a0} replaced by m_a), we obtain

$$f_a > 1.86\times 10^{8}\ \text{GeV}. \quad (34)$$

The correlations obtained in Eq. (32) and constraints on f_a as in Eqs. (33) and (34) are evidently weaker than the other restrictions shown in the previous section and obeyed by the allowed parameter space in the respective cases. The constraint in Eq. (31) is however significant in the context of gravitational wave detection. As inflation can give rise to the generation of gravitational waves through tensor perturbations, the generation of tensor perturbations during inflation is directly correlated with the Hubble parameter [66] as

$$r = 1.6\times 10^{-5}\left(\frac{\mathcal{H}_{\rm inf}}{10^{12}\ \text{GeV}}\right)^2, \quad (35)$$

which can be translated in our scenario as

$$r < 1.34\times 10^{-12}\left(\frac{f_a}{10^{13}\ \text{GeV}}\right)^2, \quad (36)$$

which is very small number to be predicted in near future as the current observational constraint on the tensor mode, $r \lesssim 0.1$, is derived from the Planck measurements of the CMB [67].

VI. CONCLUSION

Axionlike particles are well motivated dark matter candidates, which are thought to be produced primarily through the misalignment mechanism in the early Universe. In this study, we have explored the impact of electroweak symmetry breaking on the evolution of such ALP DM in presence of an explicit shift symmetry breaking dimension-6 Higgs portal interaction of it. We observe that such an operator may significantly contribute to the ALP mass during the EWSB which further initiates a change in the oscillation frequency, thereby deviating from the standard misalignment mechanism in terms of final outcome. We have shown that depending on the standard ALP oscillation temperature (which is determined by the ALP mass originating from nonperturbative dynamics only), the change in the ALP mass across EWSB gives rise to a significant modifications in relic-density allowed parameter space compared to the standard misalignment mechanism.

Our findings can be broadly categorised into two: (a) one in which we obtain an extended parameter space (in $m_a - f_a$ plane) compared to the standard misalignment mechanism, applicable when the nonperturbative mass of ALP m_{a0} exceeds 10^{-13} GeV and (b) secondly, where we obtain a parameter space with a different slope (in $m_a - f_a$ plane) compared to the standard one which applies when m_{a0} falls below 10^{-13} GeV.

Finally, taking into account all the existing constraints from several terrestrial experiments, astrophysical, and cosmological bounds on the $m_a - g_{a\gamma\gamma}$ plane (translated from $m_a - f_a$ plane) characterizing ALP's interaction with photons, we have identified a significant residue of newly opened up parameter space (from relic satisfaction point of view) in the sub-keV ALP mass regime to be compatible as nonthermal dark matter. These constraints also play a crucial role in restricting the lower limit on the cutoff scale Λ (as evident from Fig. 8), thereby forbidding the other possibility of ALP production via freeze-in from the decay or annihilations of the Higgs boson, which requires relatively smaller values of $\Lambda(\lesssim \mathcal{O}(10^9)\ \text{GeV})$. Interestingly, the predicted ALP-photon couplings turn out to be notably larger compared to the case of conventional misalignment, opening up opportunities for exploration through upcoming experiments.

ACKNOWLEDGMENTS

The work of A. S. is supported by the Grants No. CRG/2021/005080 and No. MTR/2021/000774 from SERB, Govt. of India.

APPENDIX A: ORIGIN OF DIMENSION-6 OPERATOR

Here, we present a possible origin of dimension-6 global $U(1)$ symmetry breaking operator of our kind using the fact that any global symmetry is expected to be explicitly broken by gravity at $M_{\rm Pl}$ [34–38]. For this purpose, we consider the following Lagrangian (relevant part only):

$$-\mathcal{L} \supset \mu\Phi^2 e^{i\alpha}\zeta + \frac{|H|^4\zeta^\dagger}{M_{\rm Pl}} + \text{H.c.} \quad (A1)$$

Here, Φ is our $U(1)$ symmetry breaking complex scalar field having charge $+1$ under $U(1)$, while ζ is a heavy (mass M_ζ) complex SM singlet scalar field carrying charge -2 such that the first term respects the $U(1)$ symmetry. The dimensionful coupling μ can naturally be of order $M_{\rm Pl}$. The second term being a dimension-5 operator can be thought of a soft symmetry breaking one resulting due to the explicit breaking of the $U(1)$ by gravity at $M_{\rm Pl}$. Considering the hierarchy of mass scales as: $M_\zeta < \mu = M_{\rm Pl}$, integrating out the heavy field ζ at energies below M_ζ results into the following dimension-6 term [68]:

$$\frac{1}{M_\zeta^2}|H|^4\Phi^2 e^{i\alpha} + \text{H.c.} \tag{A2}$$

Identifying M_ζ with the scale Λ, we obtain the operator considered in our analysis. Note that such a construction would not allow any other dimension-6 operator such as $\frac{|H|^2}{\Lambda^2}\Phi^4 e^{i\alpha} + \text{H.c.}$, which could otherwise be present.

APPENDIX B: PHENEMENOLOGY IN THE PRESENCE OF TWO DIMENSION-6 OPERATORS

For completeness purpose, we shall briefly discuss here how the phenomenology changes if we include the other possible dimension-6 operator (i.e., without restricting to the possible origin of such operator as outlined in Appendix A),

$$y\frac{|H|^2}{\Lambda^2}\Phi^4 e^{i\alpha} + \text{H.c.}, \tag{B1}$$

where y is a dimensionless coupling. With both the explicit breaking terms present [via Eqs. (12) and (B1)] and considering $\alpha = \pi$, ALP will acquire a bigger mass [in comparison to Eq. (16)] after EWSB, without altering the potential minimum ($\theta_{\rm min} = 0$), as follows:

$$m_a^2 = m_{a0}^2 + \frac{v^4}{\Lambda^2} + \frac{4yf_a^2v^2}{\Lambda^2}. \tag{B2}$$

Apart from inducing a sizeable contribution to the final mass of ALP, the new term [Eq. (B1)] also allows a dominant production of ALPs through decay (and annihilation) of the Higgs field after EWSB. As a result, a possible freeze-in production of ALPs remains viable in addition to the production through misalignment mechanism. Such a possibility although prevails with the other dimension-6 operator (we comment on this in the conclusion section), here with the additional one via Eq. (B1), the freeze-in of ALP may proceed with larger coupling strength (between two ALPs and the Higgs field) proportional to vf_a^2/Λ^2, in contrary to the other case [with Eq. (12) only], where f_a was replaced by the Higgs vev v ($f_a \gg v$). Hence, freeze-in can be significantly enhanced by inclusion of the operator in Eq. (B1). Additionally, it

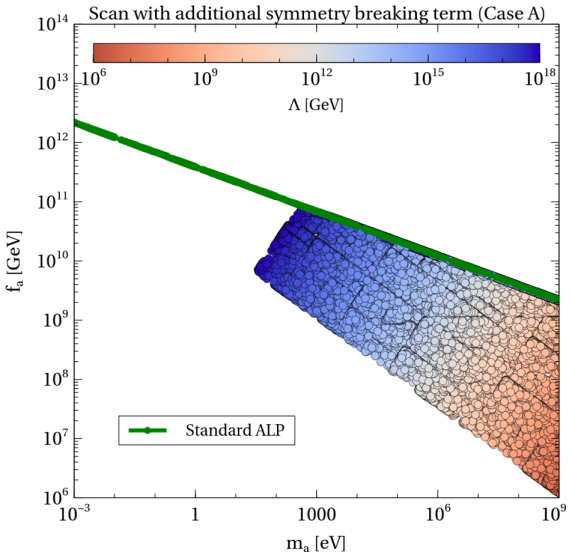

FIG. 9. Relic satisfied parameter space comparison between case A ($T^0_{\rm osc} \leq T_{\rm EW}$) and standard case in ($m_a - f_a$) plane in presence of two dimension-6$U(1)$ breaking terms. Here, the variation of Λ is shown in the color bar and $y = 10^{-4}$ is employed.

may lead to the possibility of ALP thermalization if vf_a^2/Λ^2 happens to be of order $\mathcal{O}(10^{-6})$ or more. To alleviate such possibilities, we find that restricting y by $y \lesssim \mathcal{O}(10^{-4})$, ALP can favorably be produced through misalignment mechanism only.

Therefore, considering the presence of both the dimension-6 operators with $y \lesssim \mathcal{O}(10^{-4})$, we showcase the relic allowed parameter space in Fig. 9. Here, $m_{a0} > \mathcal{O}(10^{-13})$ GeV is taken so that the conventional ALP oscillation starts prior to EWSB. As the operator of Eq. (B1) adds a substantial contribution to ALP mass via Eq. (B2), a lower value of f_a is required to achieve the correct relic density as evident from Eq. (23), which is also observed in Fig. 9. We notice that with the choice of $y = 10^{-4}$, the relic allowed parameter space is shifted beyond $m_a \gtrsim \mathcal{O}(100)$ eV, where the leftmost boundary is dictated by the choice of $\Lambda < M_{\rm Pl}$. Hence, it turns out that after imposing all the relevant cosmological and astrophysical bounds (as outlined in Sec. IV), only a tiny fraction of the parameter space remains viable to achieve the correct relic density through misalignment mechanism in this case.

APPENDIX C: TRANSITION OF ALP MASS ACROSS EWSB

In connecting the evolution of the ALP field θ across $T_{\rm EW}$, an apparent discontinuity is felt due to the sudden change in the mass of ALP: from m_{a0} at $T < T_{\rm EW}$ to m_a at $T = T_{\rm EW}$ (representative of a step function at $T_{\rm EW}$). To retain the continuity of the ALP field while passing through the EWPT, we propose to make the transition of

m_{a0} to m_a a smooth one by introducing logistic function for the mass $m_a(T)$ [69] defined as

$$m_a(T) = m_{a0} + \frac{m_a(T) - m_{a0}}{1 + e^{-2\kappa(T_{\rm EW} - T)}}, \tag{C1}$$

across $T = T_{\rm EW}$. Here, κ is a parameter which controls the abruptness involved in the transition (a large κ indicates a more sharper transition). Since the EWPT happens within a finite range of temperature ΔT, such an approximation is justified provided the change of ALP mass extends over that period ΔT. A schematic presentation of such an approximation is exhibited in Fig. 10 with $\kappa = 1$ is employed. This is for the illustration purpose in case one tries to track the evolution of the θ field via Eq. (19). While evaluating the energy density of the ALP field, we use the sudden approximation in line with Eq. (20).

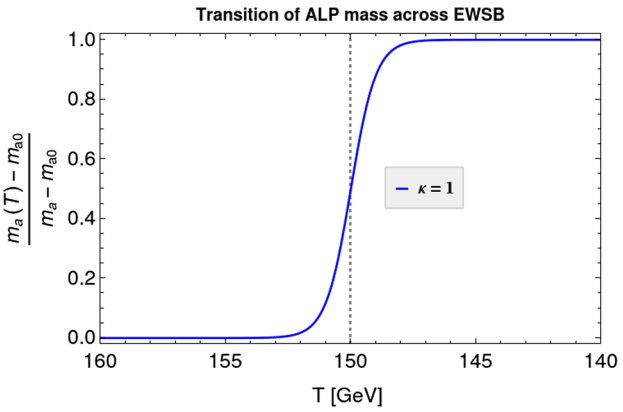

FIG. 10. Transition of ALP mass across $T_{\rm EW} = 150$ GeV with $\kappa = 1$. The dashed gray gridline corresponds to $T = T_{\rm EW}$.

[1] P. Svrcek and E. Witten, J. High Energy Phys. 06 (2006) 051.
[2] A. Arvanitaki, S. Dimopoulos, S. Dubovsky, N. Kaloper, and J. March-Russell, Phys. Rev. D **81**, 123530 (2010).
[3] M. Demirtas, C. Long, L. McAllister, and M. Stillman, J. High Energy Phys. 04 (2020) 138.
[4] R. D. Peccei and H. R. Quinn, Phys. Rev. Lett. **38**, 1440 (1977).
[5] R. D. Peccei and H. R. Quinn, Phys. Rev. D **16**, 1791 (1977).
[6] S. Weinberg, Phys. Rev. Lett. **40**, 223 (1978).
[7] F. Wilczek, Phys. Rev. Lett. **40**, 279 (1978).
[8] J. Preskill, M. B. Wise, and F. Wilczek, Phys. Lett. **120B**, 127 (1983).
[9] L. F. Abbott and P. Sikivie, Phys. Lett. **120B**, 133 (1983).
[10] M. Dine and W. Fischler, Phys. Lett. **120B**, 137 (1983).
[11] M. S. Turner, Phys. Rev. D **28**, 1243 (1983).
[12] P. Arias, D. Cadamuro, M. Goodsell, J. Jaeckel, J. Redondo, and A. Ringwald, J. Cosmol. Astropart. Phys. 06 (2012) 013.
[13] D. Cadamuro and J. Redondo, J. Cosmol. Astropart. Phys. 02 (2012) 032.
[14] A. Ringwald, Phys. Dark Universe **1**, 116 (2012).
[15] R. L. Workman *et al.* (Particle Data Group), Prog. Theor. Exp. Phys. **2022**, 083C01 (2022).
[16] D. J. E. Marsh, in *Proceedings of the 13th Patras Workshop on Axions, WIMPs and WISPs* (Verlag Deutsches Elektronen-Synchrotron, Thessaloniki, Greece, 2018), pp. 59–74.
[17] K. S. Jeong, K. Matsukawa, S. Nakagawa, and F. Takahashi, J. Cosmol. Astropart. Phys. 03 (2022) 026.
[18] H.-J. Li, arXiv:2307.09245.
[19] A. Chatrchyan, C. Eröncel, M. Koschnitzke, and G. Servant, J. Cosmol. Astropart. Phys. 10 (2023) 068.
[20] R. T. Co, L. J. Hall, and K. Harigaya, Phys. Rev. Lett. **124**, 251802 (2020).
[21] C.-F. Chang and Y. Cui, Phys. Rev. D **102**, 015003 (2020).
[22] R. T. Co, L. J. Hall, and K. Harigaya, J. High Energy Phys. 01 (2021) 172.
[23] C. Eröncel, R. Sato, G. Servant, and P. Sørensen, J. Cosmol. Astropart. Phys. 10 (2022) 053.
[24] W. Chao, M. Jin, H.-J. Li, and Y.-Q. Peng (2022).
[25] S. H. Im and K. S. Jeong, Phys. Lett. B **799**, 135044 (2019).
[26] P. S. B. Dev, F. Ferrer, Y. Zhang, and Y. Zhang, J. Cosmol. Astropart. Phys. 11 (2019) 006.
[27] V. K. Oikonomou, Phys. Rev. D **107**, 064071 (2023).
[28] D. J. E. Marsh, Phys. Rep. **643**, 1 (2016).
[29] M. Bauer and T. Plehn, *Yet Another Introduction to Dark Matter: The Particle Physics Approach*, Vol. 959 of Lecture Notes in Physics (Springer, New York, 2019).
[30] C. Balázs *et al.*, J. Cosmol. Astropart. Phys. 12 (2022) 027.
[31] T. Higaki, K. S. Jeong, N. Kitajima, and F. Takahashi, J. High Energy Phys. 06 (2016) 150.
[32] P. Draper, I. G. Garcia, and M. Reece, in *Proceedings of the US Community Study on the Future of Particle Physics (Snowmass 2021)* (American Physical Society, 2022).
[33] C. Cordova, K. Ohmori, and T. Rudelius, J. High Energy Phys. 11 (2022) 154.
[34] S. B. Giddings and A. Strominger, Nucl. Phys. **B307**, 854 (1988).
[35] S. R. Coleman, Nucl. Phys. **B310**, 643 (1988).
[36] S.-J. Rey, Phys. Rev. D **39**, 3185 (1989).
[37] L. F. Abbott and M. B. Wise, Nucl. Phys. **B325**, 687 (1989).
[38] E. K. Akhmedov, Z. G. Berezhiani, and G. Senjanovic, Phys. Rev. Lett. **69**, 3013 (1992).
[39] N. Arkani-Hamed, L. Motl, A. Nicolis, and C. Vafa, J. High Energy Phys. 06 (2007) 060.
[40] E. W. Kolb and M. S. Turner, *The Early Universe* (Westview Press Inc., 1990), Vol. 69, ISBN 978-0-201-62674-2.
[41] C. Abel *et al.*, Phys. Rev. Lett. **124**, 081803 (2020).

[42] M. Kamionkowski and J. March-Russell, Phys. Lett. B **282**, 137 (1992).
[43] R. Holman, S. D. H. Hsu, T. W. Kephart, E. W. Kolb, R. Watkins, and L. M. Widrow, Phys. Lett. B **282**, 132 (1992).
[44] S. M. Barr and D. Seckel, Phys. Rev. D **46**, 539 (1992).
[45] N. Aghanim *et al.* (Planck Collaboration), Astron. Astrophys. **641**, A6 (2020); **652**, C4(E) (2021).
[46] J. Jaeckel and A. Ringwald, Annu. Rev. Nucl. Part. Sci. **60**, 405 (2010).
[47] M. S. Turner, Phys. Rep. **197**, 67 (1990).
[48] G. G. Raffelt, Lect. Notes Phys. **741**, 51 (2008).
[49] A. Ayala, I. Domínguez, M. Giannotti, A. Mirizzi, and O. Straniero, Phys. Rev. Lett. **113**, 191302 (2014).
[50] P. Sikivie, Phys. Rev. Lett. **51**, 1415 (1983); **52**, 695(E) (1984).
[51] V. Anastassopoulos *et al.* (CAST Collaboration), Nat. Phys. **13**, 584 (2017).
[52] P. Gondolo and G. G. Raffelt, Phys. Rev. D **79**, 107301 (2009).
[53] S. De Panfilis, A. C. Melissinos, B. E. Moskowitz, J. T. Rogers, Y. K. Semertzidis, W. Wuensch, H. J. Halama, A. G. Prodell, W. B. Fowler, and F. A. Nezrick, Phys. Rev. Lett. **59**, 839 (1987).
[54] W. Wuensch, S. De Panfilis-Wuensch, Y. K. Semertzidis, J. T. Rogers, A. C. Melissinos, H. J. Halama, B. E. Moskowitz, A. G. Prodell, W. B. Fowler, and F. A. Nezrick, Phys. Rev. D **40**, 3153 (1989).
[55] C. Hagmann, P. Sikivie, N. S. Sullivan, and D. B. Tanner, Phys. Rev. D **42**, 1297 (1990).
[56] S. J. Asztalos *et al.* (ADMX Collaboration), Phys. Rev. D **69**, 011101 (2004).
[57] M. Regis, M. Taoso, D. Vaz, J. Brinchmann, S. L. Zoutendijk, N. F. Bouché, and M. Steinmetz, Phys. Lett. B **814**, 136075 (2021).
[58] J. Redondo and A. Ringwald, Contemp. Phys. **52**, 211 (2011).
[59] K.-S. Isleif (ALPS Collaboration), Moscow Univ. Phys. Bull. **77**, 120 (2022).
[60] E. Masso and R. Toldra, Phys. Rev. D **52**, 1755 (1995).
[61] J. M. Overduin and P. S. Wesson, Phys. Rep. **402**, 267 (2004).
[62] P. F. Depta, M. Hufnagel, and K. Schmidt-Hoberg, J. Cosmol. Astropart. Phys. 05 (2020) 009.
[63] C. O'hare, *cajohare/AxionLimits: AxionLimits* (2020), https://cajohare.github.io/AxionLimits/.
[64] J. Hamann, S. Hannestad, G. G. Raffelt, and Y. Y. Y. Wong, J. Cosmol. Astropart. Phys. 06 (2009) 022.
[65] M. Beltran, J. Garcia-Bellido, and J. Lesgourgues, Phys. Rev. D **75**, 103507 (2007).
[66] M. Kawasaki, E. Sonomoto, and T. T. Yanagida, Phys. Lett. B **782**, 181 (2018).
[67] P. A. R. Ade *et al.* (Planck Collaboration), Astron. Astrophys. **594**, A20 (2016).
[68] Q. Bonnefoy, Phys. Rev. D **108**, 035023 (2023).
[69] P. Di Bari, D. Marfatia, and Y.-L. Zhou, Phys. Rev. D **102**, 095017 (2020).